Towards an Energetic Modeling of Rotorcraft Using Bond-Graphs

Zeineb Chikhaoui, Julien Gomand, François Malburet, Marilena Pavel, Pierre-Jean Barre

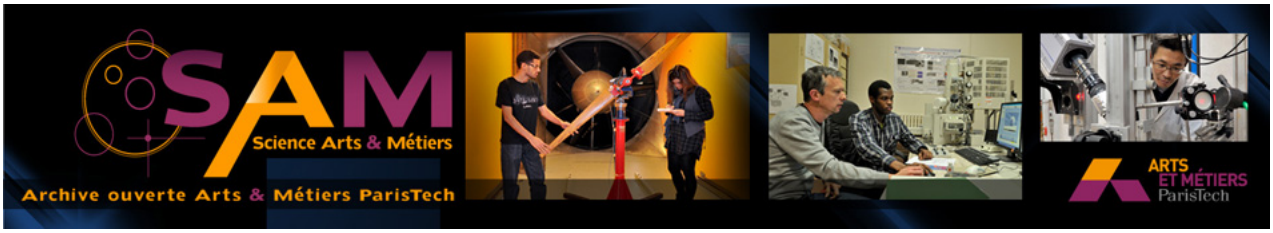

Towards an Energetic Modeling of Rotorcraft Using Bond-Graphs

Zeineb Chikhaoui
Zeineb.Chikhaoui@ensam.eu
PhD Student
Arts et Metiers ParisTech;
CNRS, LSIS
Aix-en-Provence, France

Julien Gomand
Julien.Gomand@ensam.eu
Associate Professor
Arts et Metiers ParisTech;
CNRS, LSIS
Aix-en-Provence, France

François Malburet
Francois.Malburet@ensam.eu
Associate Professor
Arts et Metiers ParisTech;
CNRS, LSIS
Aix-en-Provence, France

Marilena D. Pavel
M.D.Pavel@tudelft.nl
Associate Professor
Delft University of Technology
Delft, The Netherlands

Pierre-Jean Barre
Pierre-Jean.Barre@ensam.eu
Professor
Arts et Metiers ParisTech;
CNRS, LSIS
Aix-en-Provence, France

ABSTRACT

The paper presents an energetic method of helicopters dynamics analysis to study the air resonance (AR) phenomena. First, a brief state of art of AR phenomena is presented and a simple energetic explanation is given. Then part of the state of art is devoted to the Bond Graph (BG) and Multi-Bond Graphs (MBG) modeling method showing several advantages of the tool and few examples of MBG researches applications. This work proposes a macroscopic energetic description of a helicopter through the Word Bond Graph representation. The MBG is then used for Rotor/fuselage structure modeling in order to study the AR phenomena instability. The MBG model results are presented and show the potential of the MBG method to predict such a complex phenomenon.

NOTATION

f	= force on the blade due to shaft motion (N)
F_{bl}	= force on the blade due to lead-lag motion (N)
F_{xr}, F_{yr}	= force on the hub due to lead-lag motion (N)
	= force on the blade due to lead-lag motion (N)
M	= lead-lag moment due to the longitudinal/lateral shaft motion (Nm)
p,q,r	= helicopter roll, pitch and yaw rates (deg/sec)
x_{sh}	= shaft longitudinal displacement (m)
ζ	= lead lag degree of freedom (rad)
ω_ζ	= natural lead-lag frequency (rad/sec)
Ω	= rotor rotational speed (rad/sec)
ψ	= blade azimuth angle (rad)

INTRODUCTION

Rotorcraft are complex systems and are thus sources of recurring (especially for many new design projects) and not so well understood problems. Considering a specific phenomenon, implying interactions between many subsystems, the analysis of the system from a global but "sufficiently" detailed point of view becomes necessary. However, analyzing the whole system remains a quite difficult task. This is mainly due to:

- The composition of the system from several subsystems with multiple interactions combined with a separately-built knowledge of each subsystem, generally owned by separate company divisions, leads to a difficult global analysis of the numerous relations between system components and their environment;
- The multidisciplinary nature of the subsystems: numerous subsystems include parts related to many fields of physics (e.g. mechanics, hydraulics, aerodynamics…), and this superposition of different technologies is generally associated with the use of many different modeling tools.

Designing such complex systems may be a difficult task and requires a system approach. Physical models are essential so as to predict the system dynamic behavior. They should be available in different stages of design and should be consistent enough, i.e. with the required accuracy to deal with the specific considered problem.

Usual global modeling methodologies are mainly based on a subsystem-by-subsystem approach. The implication of different design teams, each one addressing specific disciplines, results in the use of different modeling methods and tools. The resulting global transfer functions, one for

Presented at the AHS 69th Annual Forum, Phoenix, Arizona, May 21–23, 2013.

each subsystem, are assembled in a global model through classical block diagrams as a common language. This generally leads to a mathematical view of each subsystem (e.g. for a position controller design the system's response to a specific input is analyzed to identify equivalent transfer functions between control inputs and output positions), without any energetic consideration, and usually causes loss of the link with physical equations and the associated modeling assumptions. It follows that engineers working in multidisciplinary fields need complementary tools to support complex multiphysics systems modeling in such a way as to have unified descriptions, preserving dominant physical parameters and highlighting power transfers between subsystems and, within each subsystem, between elements.

This work is part of the "Complex Mechanical Systems Dynamics" project, funded by the European Aeronautic Defense and Space (EADS) foundation. This project focuses specifically on helicopters dynamics and has as main objective to work on methodologies and analysis tools which may facilitate understanding of complex dynamic phenomena and may support or facilitate design and control activities. The present paper introduces the so-called "Bond-Graph" energetic approach of modeling, and applies it to conventional single main and tail rotor helicopters. The long-term ambitions of the project are to obtain a unified as complete as possible helicopter description, giving the ability to go from a global vision to details of subsystems dynamic behaviors - according to specific needs - and to address innovative rotorcraft architectures predesign.

The Bond Graph (BG) technique was invented in 1959 by Professor Henry Paynter of the Massachusetts Institute of Technology to model dynamic systems of multidisciplinary nature [1]. A bond graph consists in a graphical representation of a system dynamic behavior, depicting exchanges of power between basic elements such as inertia, compliances, dissipations, conservative power transformations, gyrator actions and sources. Since their invention, Bond Graphs have been applied to various fields of physics, such as thermodynamics, chemistry, biology, electronics, acoustics, solar and nuclear systems, and economics [1], [2] and [3].

The main objective of this paper is to initiate a first step towards a different vision of helicopters dynamics analysis through an application of Bond Graph methodology to well-known helicopter flight dynamics phenomena: air resonance phenomena.

The air resonance (AR) phenomena are aeroelastic instabilities that occur in hingeless (rigid) and bearingless rotors due to couplings between the rotor lead-lag motion, pitch and roll motions of the body and rotor flap regressing mode. Air resonance is usually not a problem in articulated rotor systems since they have low flapping stiffness and corresponding low body natural frequencies. The air resonance possibility for a rigid rotor exists because the relatively high rotor stiffness causes body pendulum modes to occur at frequencies which are sufficiently high to couple with the lead-lag mode. The dynamic characteristics of AR modes are complex functions of the blade flapping stiffness, rotor inertia, body inertial properties, and rotor aerodynamics [4], [5] and [6] A simple perturbation, e.g. caused by a pilot action on cyclic controls or a wind gust on the fuselage, can lead to instability appearing mainly in the aircraft roll motion [7]. AR can be solved by increasing the damping levels. This may be accomplished through: 1) the use of lag dampers, however this results in extra weight, 2) introducing aeroelastic couplings in the rotor [6] resulting in "damperless" configurations. However, understanding the role of aeroelastic couplings in AR as a mean to prevent this instability is complex and although much progress has been made, AR is still a complex and difficult to predict aeroelastic instability.

This paper is organized as follows. Section 2 is devoted to the description of a usual simple energetic approach to understand the AR phenomenon, and to a short introduction to Bond Graphs. Section 3 proposes an energetic modeling of part of a single main and tail rotor helicopter using BG. Then, in Section 4, the proposed BG model is validated through a comparison with classical analytical modeling results, and simulation results are exposed, using 20-Sim software, to illustrate its capability to predict real dynamic phenomena such as air resonance. Finally concluding remarks are given and directions for future research are proposed.

STATE OF THE ART

This section first presents how air resonance (AR) can be predicted using a simple energetic explanation. Then, key elements of the BG methodology are given, and expected advantages of this tool, according to the project objectives, are exposed.

A Simple Energetic Approach to understand the Air Resonance Phenomenon

Energy is one of the fundamental concepts in science and in this way it is useful to understand the behavior of complex dynamic systems through the energies accumulated into their subsystems and the flow of energies between the sub-bodies. Ambitions in the present part are oriented first towards a simple explanation of AR phenomena with an energetic vision.

There are numerous air resonance related publications. Early research work has been carried out by [8], he gives an introduction to helicopter Air Resonance and gives a simple theoretical treatment of the phenomena. Others work dealing with instability due rotor/structure coupling, taking examples of Air/ground resonance [7], [9], [10] and [11].

The usual provided solution for this problem is purely mechanical employed in the design phase. It consists on adapting the according stiffness and damper for the lag motion of the blade, in order to obtain different eigenfrequency on flap and lag axis [6].

Global objectives of our research are to demonstrate first capability of the BG method to predict this phenomenon.

First, a simple energetic understanding of the AR problem is given. The approach used next is the so-called "energy flow" method and is a semi-qualitative method primarily based on BG [12]. The main idea of energy flow method is that any instability possesses a multiplicity of energy flow paths (vicious circles) in which energy is transferred from one degree of freedom to the other. The method follows the steps:

1- The dynamical equations of motion are written as a set of second-order systems;

2- Each degree of freedom (DOF) is considered as an excitation for the other DOF. Therefore, the coupling terms are external excitations for each separate degree of freedom;

3- It is assumed that there is "virtual" damping in each degree of freedom such that an oscillation with constant amplitude results. The amount of damping does not depend on the actual damping;

4- Next, one inspects whether there are any external excitations (coupling terms) in phase with the velocity of the degree of freedom considered. If so, the coupling term - "excitation" - pumps energy into or extracts energy from the DOF.

5- If there are degrees of freedom which mutually pump energy into each other, this indicates the possibility of dynamic instability. The reasoning here is that the added virtual damping must continuously dissipate energy to achieve the constant amplitude. If the actual damping is less, then the mutual energy exchange would tend to increase the motion amplitude.

Usually, the AR instability is plotted in the so-called air resonance diagram, see Figure 1. This diagram gives the frequency of the lead-lag blade mode as seen in the nonrotating body frame as given by regressing lead-lag mode $\left|\Omega-\omega_\zeta\right|$ and advancing lead-lag mode $\left|\Omega+\omega_\zeta\right|$ as a function of rotor rpm. One can see the AR region where the body roll and/or pitch mode intersects the regressing lead-lag mode. In the figure one can also see the representation of the "ground resonance" phenomenon, the equivalent of AR problem when the helicopter is grounded. For a soft in-plane rigid rotor (characterized by the rotating first lead-lag frequency lower than 1P, $\omega_\zeta<\Omega$), a critical body frequency coincides with the regressing lead-lag frequency if the rotor over-speeds while on ground, and in air resonance if the rotor is slowed in flight. It is usually stated in the literature that, for a rigid rotor, no driving energy is available in the region to the left of $\Omega=\omega_\zeta$, whereas to the right of this point the existence of a source of driving energy is indicated [4]. Thus, a soft in-plane rotor is prone to ground and air resonance.

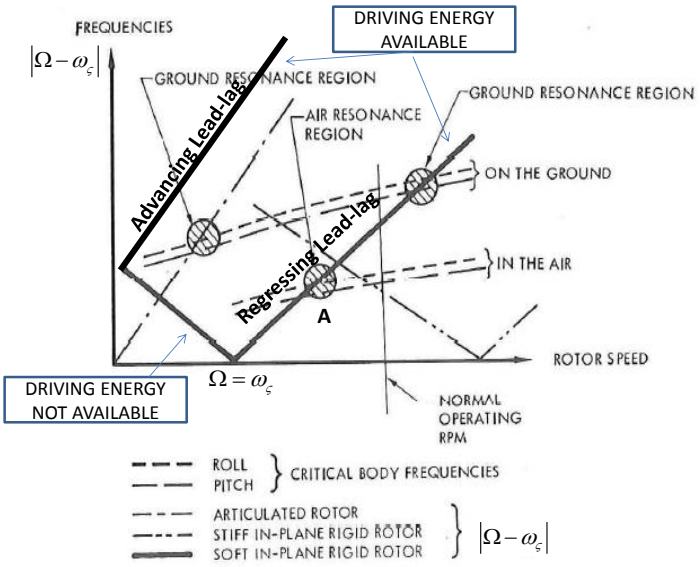

Figure 1. Diagram ground and air resonance [adapted from 4]

Next paragraph will demonstrate by using energy flow diagram that indeed, point A in Figure 1 is dangerous for instability, describing how the vicious circle of instability is closed. The following simplified model is used (see Figure 2). It consists of a constant speed shaft (angular velocity ψ) which may translate longitudinally and laterally w.r.t. an inertial frame. A hub is connected to the shaft by means of a spring K_ζ, so that the hub may have a variable angular velocity $\Omega+\dot{\zeta}$. To the hub is attached a massless beam with a concentrated mass m at its end. In order to balance the average centrifugal force, a counterweight is attached to the shaft. For the moment, the blade flapping motion is not included in the model as point A in Figure 1 is not giving explicitly the importance of flap motion in AR problem.

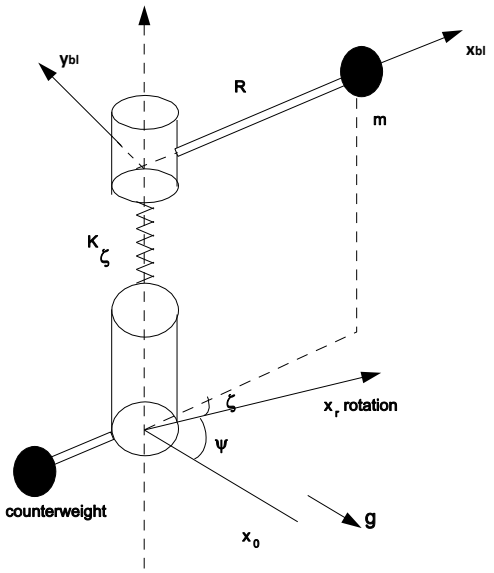

Figure 2. Simplified model to represent the rotor/body motion

The angular velocity of the blade is:

$$\underline{\omega}_{bl} = (0,0,\Omega+\dot{\varsigma})\{\underline{E}_{bl}\} \tag{1}$$

The absolute displacement of the blade:

$$\underline{r} = R(1,0,0)\{\underline{E}_{bl}\} \tag{2}$$

The absolute velocity:

$$\dot{\underline{r}} = R(1,0,0)\left\{\dot{\underline{E}}_{bl}\right\} = R(1,0,0)[\omega_{blx}]\{\underline{E}_{bl}\} \tag{3}$$

where $[\omega_{blx}]$ represents the matrix time derivative of the unit vector

$$\{\dot{\bar{E}}\} = \begin{bmatrix} 0 & r & -q \\ -r & 0 & p \\ q & -p & 0 \end{bmatrix}\{\bar{E}\}$$

that is in our case:

$$[\omega_{blx}] = \begin{bmatrix} 0 & \Omega+\dot{\varsigma} & 0 \\ -(\Omega+\dot{\varsigma}) & 0 & 0 \\ 0 & 0 & 0 \end{bmatrix}$$

The absolute acceleration:

$$\ddot{\underline{r}} = R(1,0,0)[\dot{\omega}_{bl}]\{\underline{E}_{bl}\} + R(1,0,0)[\omega_{blx}]^2\{\underline{E}_{bl}\} = R\left(-(\Omega+\dot{\varsigma})^2, \ddot{\varsigma}, 0\right)\{\underline{E}_{bl}\} \tag{4}$$

The force due to the "lead-lagging" mass on the hub is then:

$$\underline{F}_{bl} = (F_x, F_y, 0)\{\underline{E}_{bl}\} \tag{5}$$

According to D'Alembert principle1, this means the inertial forces:

$$\begin{aligned} F_x &= mR(\Omega+\dot{\varsigma})^2 \\ F_y &= -mR\ddot{\varsigma} \end{aligned} \tag{6}$$

Lead-lag moment equation:

$$-F_y R + K_\varsigma \varsigma = 0 \tag{7}$$

$$\ddot{\varsigma} + \omega_\varsigma^2 \varsigma = 0 \tag{8}$$

with $\omega_\varsigma = \sqrt{\dfrac{K_\varsigma}{mR^2}}$.

The force on the shaft, taking into account the extra counter-weight is:

$$\underline{F}_r = (F_x, F_y, 0)[\varsigma]\{\underline{E}_r\} - mR\Omega^2(1,0,0)\{\underline{E}_r\} \tag{9}$$

With $[\varsigma] = \begin{bmatrix} \cos\varsigma & \sin\varsigma & 0 \\ -\sin\varsigma & \cos\varsigma & 0 \\ 0 & 0 & 1 \end{bmatrix}$ the rotation matrix from $\{\underline{E}_r\}$ to $\{\underline{E}_{bl}\}$; $\{\underline{E}_{bl}\} = [\varsigma]\{\underline{E}_r\}$

$$\underset{\text{Cor.}}{\underline{F}_r} \approx^{\text{linearized}} \underset{\text{Cf. Inert.}}{mR\left(2\Omega\dot{\varsigma}, \Omega^2\varsigma - \ddot{\varsigma}, 0\right)\{\underline{E}_r\}} \tag{10}$$

Case 1:

Firstly, consider the AR situation as represented by point A in Figure 1 and assume that the values of the eigenfrequencies are:

$$\begin{aligned} \omega_\varsigma &= \frac{1}{2}\Omega \\ \omega_{sh} &= \frac{1}{2}\Omega \end{aligned} \tag{11}$$

Assume an oscillatory motion:

$$\varsigma = \varsigma_0 \cos\left(\omega_\varsigma t\right) = \varsigma_0 \cos\left(\frac{1}{2}\Omega t\right) = \varsigma_0 \cos\left(\frac{\psi}{2}\right) \tag{12}$$

It follows that:

$$\dot{\varsigma} = -\varsigma_0\omega_\varsigma \sin\left(\omega_\varsigma t\right) = -\frac{1}{2}\varsigma_0\Omega\sin\left(\frac{\psi}{2}\right) \tag{13}$$

$$\ddot{\varsigma} = -\varsigma_0\omega_\varsigma^2 \cos\left(\omega_\varsigma t\right) = -\frac{1}{4}\varsigma_0\Omega^2 \cos\left(\frac{\psi}{2}\right) \tag{14}$$

First, describe the lead-lag motion as an external excitation for the shaft. The effective forces on the hub due to the blade lead-lag motion can be found by substituting (13) and (14) into equation(10):

$$\begin{aligned} F_{xr} &= 2mR\Omega\dot{\varsigma} = -mR\Omega^2\varsigma_0 \sin\left(\frac{\psi}{2}\right) \quad \text{(Coriolis)} \\ F_{yr} &= mR\left(\Omega^2\varsigma - \ddot{\varsigma}\right) = \frac{5}{4}mR\Omega^2\varsigma_0 \cos\left(\frac{\psi}{2}\right) \quad \text{(cf + inertia)} \end{aligned} \tag{15}$$

Since one investigates the system at resonance, and because the external lead-lag motion excites the shaft in a resonant point, it follows that the blade lead-lag motion gives rise to a shaft motion 90 deg phased w.r.t. the lead-lag motion. Using (12) and (15), the motion of one blade over 4 periods and the force on the shaft can be represented (each lead-lag cycle takes two revolutions) as shown in Figure 3.

One can see that, regarding the forcing terms acting on the shaft, a force will be exerted on the shaft to the right. One revolution later, at $\psi=2\pi$ maximum lag occurs with an attendant force on the shaft to the left, etc. If it is wished, this may be also checked by substituting $\zeta(\psi)$ into the equations of motion. Concluding, there is a "rotating" force acting on the shaft, against the rotor direction of rotation.

[1] D'Alembert principle allows to convert dynamic problems in static ones. Typical usage of this principle consists of representing the statement of Newton's second law F=ma by an "inertial load" equal to ma, but directed opposite to the acceleration, a.

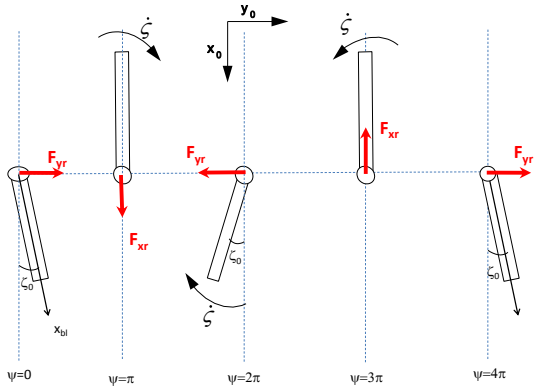

Figure 3. Lead-lag motion of one blade as external excitation for the shaft and the corresponding force on the shaft

Secondly, describe the shaft motion as an external excitation for the blades. Assume that the shaft can move only longitudinally (direction x0), being excited in its eigenfrequency $\omega_{sh} = \frac{1}{2}\Omega$. The blades will move up and down with the shaft with acceleration $\ddot{x}_{sh}$. Looking at (12), the shaft longitudinal displacement will be:

$$x_{sh} = x_{sh0}\cos(\omega_{sh} t) = x_{sh0}\cos\left(\frac{\psi}{2}\right) \tag{16}$$

D'Alembert principle will be used next to determine the force on blade due to the shaft motion:

$$f = -f_0 \cos\left(\frac{\psi}{2}\right) \tag{17}$$

and the motion of the shaft during 4 periods is now as represented in Figure 4

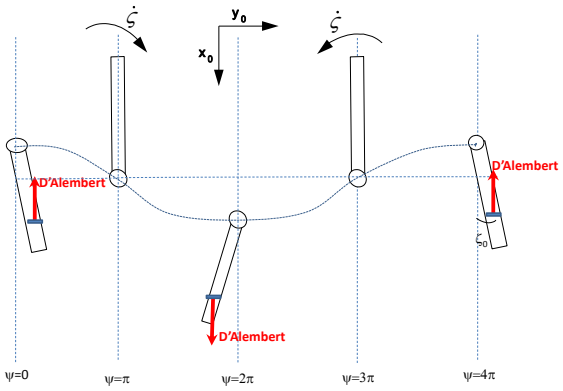

Figure 4. Longitudinal shaft motion as external excitation for the blade and the corresponding force on the blade

One can see that:

- Fxr is in phase with $\dot{x}_{sh}$, thus energy input goes in the shaft.
- An extra lead-lag moment as a result of the shaft acceleration is out of phase with $\dot{\varsigma}$, so there is no energy input from the shaft to the blade.

The extra lead-lag moment due to the longitudinal shaft motion can be calculated as:

$$M = -fR\sin(\psi+\varsigma) \overset{\text{linearized}}{\approx} f_0 R\cos\left(\frac{\psi}{2}\right)(\sin\psi + \varsigma\cos\psi) =$$

$$f_0 R\cos\left(\frac{\psi}{2}\right)\times\left(\sin\psi + \varsigma_0\cos\left(\frac{\psi}{2}\right)\cos\psi\right) = \tag{18}$$

$$f_0 R\left[\frac{1}{2}\sin\frac{3}{2}\psi + \frac{1}{2}\sin\frac{\psi}{2}\right] + f_0\varsigma_0 R\left(1+2\cos\psi+\cos 2\psi\right)$$

Equation (18) does not contain any component in phase with lag velocity(13).

Assume now that the shaft can move only laterally (direction y0). The shaft lateral displacement will be:

$$x_{sh} = x_{sh0}\sin(\omega_{sh} t) = x_{sh0}\sin\left(\frac{\psi}{2}\right) \tag{19}$$

The lateral force on blade due to the shaft motion is given according to D'Alembert principle as:

$$f = f_0 \sin\left(\frac{\psi}{2}\right) \tag{20}$$

The lateral shaft motion during 4 periods can be represented now as seen in Figure 5:

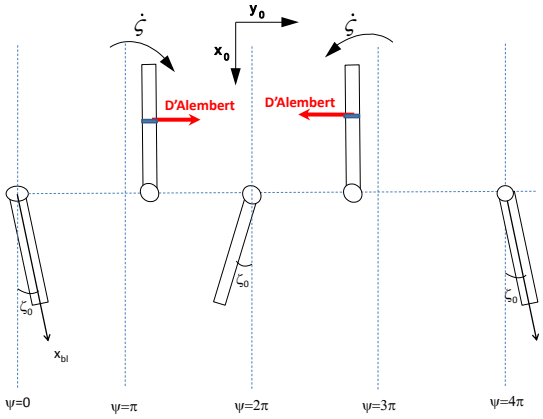

Figure 5. Lateral shaft motion as external excitation for the blade and the corresponding force on the blade

One can see that:

1- Fyr is in phase with $\dot{y}_{sh}$, so energy input goes in the shaft.

2- An extra lead- lag moment as a result of the shaft acceleration is in phase with $\dot{\varsigma}$, thus there is energy input from the shaft to the blades

The extra lead-lag moment due to the lateral shaft motion can be calculated as in (21). In this case, relation (21) does contain a component in phase with lag velocity(13). This shows that, in ground resonance (represented as an intersection point between shaft and blade lead-lag frequency in the $|\Omega - \omega_{\varsigma}|$ diagram, the lateral shaft motion combines with blade lead-lag motion.

$$M = fR\cos(\psi+\varsigma) \overset{\text{linearized}}{\approx} f_0 R \sin\left(\frac{\psi}{2}\right)(\cos\psi - \varsigma\sin\psi) =$$

$$f_0 R \sin\left(\frac{\psi}{2}\right) \times \left(\cos\psi - \varsigma_0 \cos\left(\frac{\psi}{2}\right)\sin\psi\right) = \quad (21)$$

$$f_0 R\left[\frac{1}{2}\sin\frac{3}{2}\psi - \frac{1}{2}\sin\frac{\psi}{2}\right] - f_0\varsigma_0 R\left(\frac{1}{4} - \frac{1}{4}\cos 2\psi\right)$$

The next question is what is the role of flapping motion in the AR mode? Reference [13] demonstrated that Coriolis force on the blade due to flap velocity has a destabilizing effect on the motion. If the term representing the inclination of the flapping moment w.r.t. flapping velocity would have been included in the lead-lag equation, one would found that energy is pumped from the lag motion into the flap motion. In the case of the roll-flap-lag dynamic system [13] represented the energy flow for the dynamic system as seen in Figure 6.

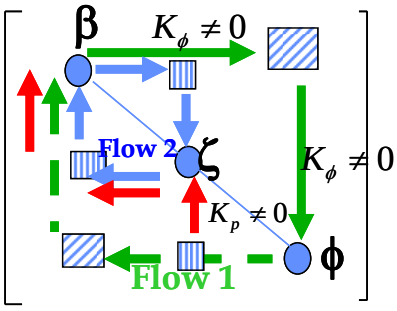

Figure 6. Energy flow in the roll-flap lag system [13]

One can see that body roll angle ϕ couples to the lead-lag motion ζ in the case when the fuselage roll rate gain Kp≠0, driving the lag motion unstable. The lag drives the flap β unstable and, as a result, the flap, in certain conditions (roll attitude gain Kϕ≠0) , flaps pumps energy into the lead-lag motion driving the AR mode unstable. , In an attempt to understand the major source of damping in the AR mode, [14] demonstrated that, in general, typical soft in-plane rotors have a powerful damping available in the flap mode (3 to 6 times that of a typical articulated rotor) which damps the roll motion and does not result in AR instability. Only when rotor flapping is modified by the influence of an external control system such as stability augmentation or gyro bar, the powerful flap damping available in such rotor modifies driving the AR mode unstable. This was the case explained by [15] for the EC135 helicopter. The authors developed an air resonance controller for the EC135 to alleviate the AR mode. According to their study it appeared that, in the basic helicopter operation condition, air resonance was not an issue for the pilots operating the EC135, the air resonance instability manifesting as a body roll oscillation which was existent but below the pilot perception level. However, when the helicopter was enhanced with an Attitude command/Attitude Hold (ACAH) control system for flying attitude command or flight path following tasks, it became apparent that, increasing too much the roll rate feedback gain, drove unstable the air resonance mode. This time the oscillation was perceived by the pilot as an oscillatory ringing in the helicopter roll response at a frequency of about 1.8Hz in the case of EC135. It was demonstrated that in this case the helicopter was PIO prone when applying the ADS-33 bandwidth criterion. In order to damp the air resonance mode when rate feedback was used, the authors developed an air resonance controller which effectively damped the coupled body-roll air resonance mode, independently from the main flight control system.

Appendix A demonstrates further using energy flow method the cases when the intersection of the body mode with the lead-lag mode is on the two other branches of the air resonance diagram. It will be shown that the circle of vicious energy is not closed and no instability can appear as concerns the AR mode.

Bond Graph Basics

The usual modeling approach based on a concatenation of equivalent transfer functions, one per subsystem, gives a mathematical view of the system, generally associated with a loss of physical sense, of dominant physical parameters, and of modeling hypotheses [16]. This way, knowledge capitalization remains a quite difficult task, and products evolutions necessitate partly starting again the modeling process. For these purposes, complementary methods, offering powerful unified modeling languages, have been designed to support and simplify complex multiphysics systems modeling and analysis, and to minimize physical misunderstood. Among these tools, Bond Graph (BG) [1] is chosen for its different interesting stages of modeling and analysis, and its ability to manage different detail levels for subsystems dynamic behavior description:

1- Bond Graphs represent energy transmission into systems through power bonds, highlighting generalized effort and flow variables - power variables - between components. In mechanical engineering, forces and torques are effort variables, while speeds are flow variables - respectively voltages and currents in electrical engineering, pressures and flows in hydraulics, etc. Each bond is represented by a half arrow and defines a bidirectional connection, so-called power bond, each direction being associated with either an effort or a flow variable [1]-[2].

2- First step in the BG methodology consists in a functional analysis of the considered system, in order to build a word description, so called word bond graph [3], of its global architecture. It consists in a decomposition of the system into subsystems and a description of their different power interactions. Each subsystem can then be described through another word BG, and so on.

3- Then, a more detailed description of each subsystem is conducted. For that, fundamental energy processes are defined by specific elements. Depending on their power function and connections, five main types of elements can be distinguished [3, 16]:
    - Energy sources ('Se', 'Sf', respectively effort and flow sources);
    - Energy accumulation elements ('I', 'C', respectively inductive and capacitive accumulators);
    - Perfect transformation ('TF', or 'MTF for modulated 'TF') elements, without energy accumulation or dissipation;
    - Perfect coupling elements for energy distribution ('0', '1', respectively for common effort and common flow junctions);
    - Dissipative elements ('R'), representing the system energy losses.
4- Finally causal analysis is carried out to generate a, so-called, causal BG model. Causalities are assigned following a sequential causality assignment procedure with specific rules [3]-[17]: Sources naturally impose their causality constraint to their nearest element. Then, integral causality is generally preferred for a natural representation of accumulation processes. However, in some cases, causality conflicts can occur and lead to the use of accumulation elements represented in a derivative form. Depending on the chosen modeling assumptions for a system, some of its energy storage elements can be partly represented with derivative causality. This can occur, for example, when a mechanical shaft is considered as a perfectly rigid element between two inertial accumulators. In this case, one can modify the modeling assumptions, taking into account the stiffness of the shaft, so as to really consider two degrees of freedom, and thus two independent inertial accumulators.

The BG methodology can thus be considered as a quite complete tool supporting, in a graphical way, the entire modeling process, from the system structural analysis to the causality assignment and assumptions management. Bond Graphs are usually classified among "energetic" modeling tools because of their ability to represent and manage power transfers, and thus to give access to energy through simple integrations. With its "word" level, the BG representation offers the possibility to evolve gradually from a macroscopic system description to a more detailed view giving access to elementary accumulation and dissipation processes. This BG property matches the multi-level representation objective of the project. In addition, each elementary process is associated with its corresponding equations so that the global system equations can be derived. Specific BG graphical rules [3] can also support model analysis and will be studied in future work.

Multi-Bond Graphs for 3D Multi-body Systems

Initially developed with a scalar form, Bond Graphs have been more recently extended to a vector form, so-called "multi-bond graph", to deal with three dimensional (3D) multi-body systems [3]. Indeed, a scalar bond graph method, as previously presented, could also be applied to multi-body systems. However, for complex systems, such scalar graph would quickly become too complicated to remain useful, and its ability to give an overall structural vision of the system would be lost. For example, [18] proposes a scalar bond graph model of a multidisciplinary nonlinear system involving multi-body system dynamics, hydraulic actuation system dynamics, and electronic controller dynamics. For the sake of clarity and efficiency, authors intend, in their future work, to convert the proposed scalar model into a multi bond representation. Thus, bond graphs have been also chosen for this project because it now provides a methodology to address 3D multi-body systems.

Multi bond graph (MBG) methodology can be seen as an extension of the classical scalar BG method. The multi-bond notation was introduced by Bonderson [19], and then improved by Breedveld [20]. In this last notation, bonds have been extended to multi-bonds representing effort and flow vectors, and scalar elementary components (dissipations, accumulations, etc.) representing fundamental energy processes were extended to the corresponding multi-port elements. Finally Tiernego and Bos [21] proposed a systemic approach to model a freely moving rigid body and Borutzky, in [3], described a multi-bond graph library with the related multi-bond notations and proposed a systematic modeling approach for moving rigid bodies and various types of mechanical joints. Then the method has been illustrated by a simple application to a planar pendulum.

Initially, the MBG method was only used to simplify the graphical representation of complex mechanical multi-body system, without causality assignment capabilities. This last operation required to explode the MBG model into its equivalent scalar BG form. This limitation has been recently issued thanks to a specific MBG causality assignment procedure. Reference [22] explains how equations of motion can be derived from a MBG through an application to a planar RRS mechanism and a spatial crank-slider mechanism.

Multi-bond graph representation of a rigid body and a mechanical joint will be illustrated in the next section devoted to helicopter multi-bond graph modeling.

A further advantage of bond graphs and multi-bond graphs is the existence of specific software, dedicated to BG and MBG models structuration, simulation and analysis. In the present study, the 20-sim software is used. This software includes a backward differentiation method, able to solve problems with numerous occurrences of derivative causalities and algebraic loops, frequently observed in multi-bond graph representations [22]-[23].

Multi-Bond Graphs Applications

Many researches show applications and advantages of multi-bond graphs (MBGs) for various objectives. Borutzky [3] presents a brief survey on MBGs including references to MBG applications, especially in robotics and automotive industry. He also pointed out applications of MBG in different areas such as human body or mobile robots modeling. Other recent papers can be cited for various applications, for example:

- In [24], authors propose a modeling of electric vehicles dynamics with MBG to facilitate dynamic behavior analysis and understanding.
- In [25], authors propose an application of vector Bond graphs to the modeling of a class of hand prostheses. They indicate that this method is useful for simulations and control design of such biomechanical systems.

Multi bond graphs have also been applied to some interesting applications in aeronautics:

- In [26], authors propose a bond graph dynamic modeling of a quad-rotor helicopter. They first present an open loop unstable model and propose closed loop controllers to ensure the rotorcraft stabilization. The rotorcraft is then controlled, from an initial roll, pitch, yaw and altitude configuration, to a desired steady state. In this paper, the BG has been chosen to facilitate model construction and troubleshooting.
- In [27], a MBG model of a scanner servo-control for the orientation of a fighter aircraft is proposed. The studied system is composed of an aircraft rigid body and a scanner, containing a gimbal box and an antenna. The azimuth and elevation movements of the scanner are controlled by servocontrols. MBG has been applied for this complex system because of its capability to integrate various physical domains (electrical, mechanical and system control) with multiple degrees of freedom. The obtained model has been used to study servocontrols on the scanner of the radar, part of a real fighter aircraft.

These two last examples illustrate advantages of multi bond graphs through their application to relatively simple aeronautic cases compared to single main and tail rotor helicopters. The first one considers the aircraft as a single freely moving rigid body to be positioned thanks to four controllable forces. This modeling assumption can be sufficient for typical drone systems, but is not adapted any more to deal with more complex helicopters in which some major subsystems and their interactions have to be considered. The second example exposes a more complex system, representing several subsystems with multiple interactions and related to many fields of physics. However, our objective is different, seeking to address instability problems which take origin in inertial couplings between several moving bodies in interaction with aerodynamics.

The BG and MBG methodology corresponds to a generic graphical description to support the development of a model, from the first chosen assumptions to simulation of the dynamic behavior for validation purpose. Furthermore, the scalar BG method can be used to address other issues related to control design such as, for example, analysis of controllability and observability structural properties [3]. Thus, the first steps exposed in this paper consists in using MBG to model part of a single main and tail rotor helicopter and in illustrating its ability to predict known phenomena such as air resonance. Future ambitions will be oriented to investigate the potential of existing scalar BG analysis methods in application to MBG models and to exploit MBG graphical form for controller design objectives.

MULTI-BOND GRAPH ENERGETIC MODELING OF A HELICOPTER

This section introduces a first step toward an energetic modeling of a single main and tail rotor helicopter. First, a macroscopic energetic analysis of generic helicopter architecture is proposed to establish a macroscopic word multi bond graph, including the transmission linkage between engine power source and the two rotors. Then, the main rotor and helicopter body subsystems are considered so as to address AR phenomena. The corresponding word MBG is proposed and MBG modeling of a rigid body is explained through the example of one rigid blade model.

Macroscopic representation of a helicopter

A functional and energetic analysis is conducted to establish a word bond graph description of a classical helicopter. It consists in a decomposition of the studied system into subsystems and a description of their power interactions.

When achieving a global energetic analysis of a system, a few key questions have to be addressed first. The first one concerns the identification of energetic sources to delimitate the modeling study boundaries. From a mechanical point of view, the helicopter engine is supposed to be the main power source. Then, additional mechanical sources have to be considered to take into account interactions of the helicopter with its environment. For example, one can consider external sources corresponding to the contact with the ground or multiple interactions with environing air. In the present study, no interaction with the ground is considered. Another question concerns destinations of energy. In helicopters, energy is essentially distributed between rotors, interacting with the aerodynamic environment to generate forces applied to the helicopter body, and the control of the helicopter body motion, also interacting with its aerodynamic environment.

The chosen boundaries for the model thus appear as sources on the macroscopic word multi-bond graph depicted in Figure 7: three aerodynamic sources, respectively interacting with the body and the main and tail rotors, and one engine mechanical source.

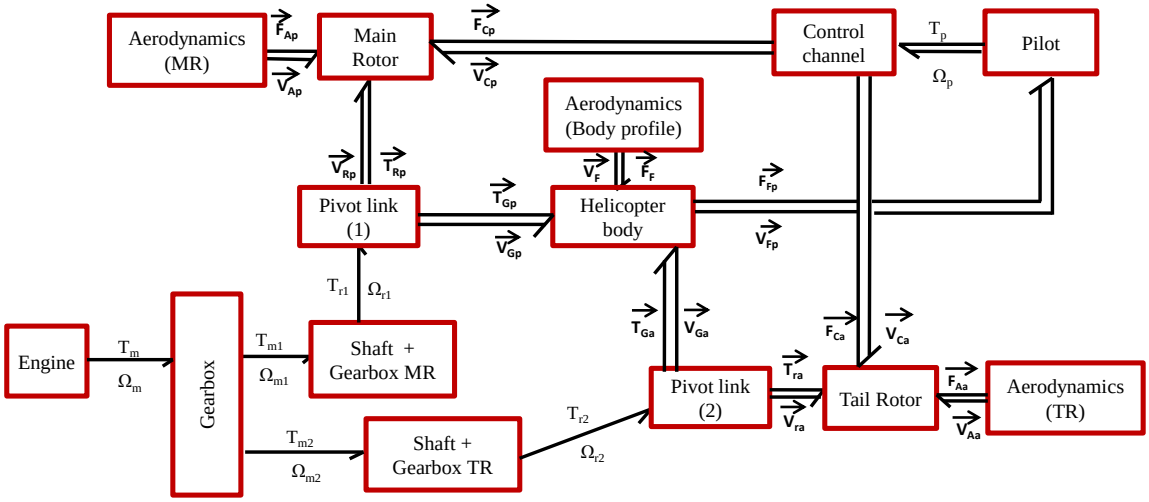

Figure 7. Macroscopic representations of helicopter dynamics in word Bond graph representation

The linkage between these sources is composed of a set of gearboxes, shafts and bell cranks, and the main and tail rotors (respectively MR and TR). These last are linked to the helicopter body through pivot joints of the MR and TR gearboxes, allowing power transmission to the fuselage. The pilot is carried by the helicopter body and interacts with the main and tail rotors through control channels.

One can note that no particular rule imposes to decompose the system with a specific or homogenous detail level of subsystems. Figure 7 illustrates this point describing engine power transmission to the two rotors through "shafts & gearboxes" subsystems associated with "pivot links". The latter, referring to a much more detailed level of description, also could be included within the "shafts & gearboxes" subsystems. In the same way, "engine", "gearboxes" and "shafts & gearboxes" could be grouped in a single more macroscopic "engine mechanical power source" subsystem with two output power bonds, while preserving the two "pivot links" representation. One can also note that both scalar and multi-dimensional power bonds are simultaneously used within the same bond graph representation: Power transmission from the engine to the two pivot links is depicted in scalar form, using classical power bonds from scalar bond graphs, while multi-bonds are required to describe power transmission between aerodynamic sources, rotors, helicopter body, pilot and control channels subsystems. Each scalar bond is thus associated with a couple of power variables, including an effort – torque – and a flow – rotating speed – variable, while multi-bonds are associated with a couple of effort and flow vectors. At this macroscopic representation level, for the sake of simplicity, both 3-dimentional rotational and translational components have been grouped into single multi-bonds. However, these 6-dimentional power bonds will be split into the corresponding two 3-dimentional power vectors when a multi-bond graph will be built for simulation purpose.

This Word BG gives an energetic macroscopic description of the helicopter and provides a methodological support to simplify analysis of power paths between subsystems. It corresponds to a first level of the desired multilevel representation of helicopters.

To address air resonance phenomena prediction through a bond graph model simulation, we will now focus on the multi-bond graph modeling of the main rotor subsystem.

Bond graph modeling of the main rotor subsystem

For this first helicopter bond graph modeling, we selected air resonance as an interesting instability phenomenon to be addressed. Indeed, this phenomenon implies complex couplings between roll and/or pitch motions and blades flap and lead-lag motions occurring in a rotating frame w-r-t the helicopter body frame. If this paper intends to demonstrate bond graph tools ability to predict such phenomena, future work ambitions are oriented towards the exploitation, through some specific properties, of bond graphs graphical and power oriented form to analyze conditions of occurrence of such phenomena since early design stages. One can also imagine exploitation of such tools for control design purpose.

Helicopter modeling activities are thus now focused on the bond graph modeling of the main rotor subsystem. The proposed model has also to include a simplified lumped parameters model of the fuselage and a relatively simple aerodynamic model. Modeling main assumptions are chosen as follows:

- The fuselage is considered as a single rigid body, described by its inertia and mass matrices, with 6 degrees of freedom.
- As the tail rotor action will not be modeled, the yaw motion is artificially blocked.

- The roll and pitch instantaneous centers of rotation are both fixed to a single point aligned with the main rotor axis and above (at 0.7 m) the rotor hub pivot joint center. The vertical position of this point is also artificially fixed to ground so as to avoid a complex search of steady flight conditions to simulate helicopter hover.
- The link between the fuselage and the main rotor pivot link is supposed to be infinitely stiff.
- The critical body frequency on the roll axis is supposed to be at 1.3 Hz and reproduced thanks to the roll term of the fuselage inertia matrix associated with the corresponding equivalent roll axis stiffness.
- The engine speed control is supposed to be perfect, so the engine mechanical source, including gearboxes ratios, is modeled by a perfect controllable rotational speed source (at 27.75 rad·s^{-1}) applied to the rotor hub whatever the load torque is.
- Blades are considered as rigid bodies, modeled by their inertia and mass matrices.

Some of these assumptions and additional notations are illustrated through Figure 8 depicting the considered lumped parameters model of the rotor-fuselage subsystem.

In the present study, we consider a four-bladed helicopter. Each of the blades is linked to the rotor hub through an equivalent ball joint. To facilitate access to the relative blade angular position signals w-r-t the hub, these joints are modeled thanks to three successive and collocated pivot links, as depicted in the rotor word multi-bond graph of Figure 9. Starting from the hub, the two first pivot joints correspond respectively to the lead-lag, ς, and the flap, β, motions of the considered blade, while the third one corresponds to its pitch angle, θ, and is controlled by the pilot. The pilot control action is modeled by three perfect modulated velocity sources, one for each of the considered helicopter control axes: two for the roll and pitch controls, acting on the cyclic blade pitch angle, and one for the collective pitch angle. These three velocity sources act on blades pitch angle through a Coleman transformation and are thus controlled by sigmoid signals so as to ensure a smooth pitch positioning. This kinematic model of the pilot and control channels subsystems is not represented in Figure 9 for the sake of simplicity.

In the word MBG of Figure 9, one can distinguish three types of multi-bond graph elements:

- Moving rigid bodies, such as the fuselage, the rotor hub and the four blades.
- Joints, such as pivot links used between the hub and the fuselage and for blades connections with the hub.
- Multi-bond graphs power bonds (half-arrows).

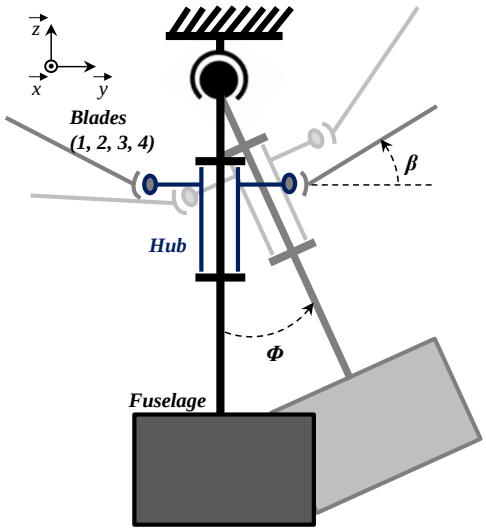

Figure 8. Lumped parameters model of the rotor-fuselage subsystem

Each joint or body element is linked to another element through two parallel power bonds, respectively for the rotational and translational power transmissions. Each power bond thus carries a three-dimensional flow (rotational or translational speeds) vector, associated with the corresponding three-dimensional effort (torques or forces) vector.

Aerodynamic lift forces F_l are applied on each blade *z*-axis as functions of both the rotor speed (Ω) and the blade pitch angle (θ), as described in (22) where ρ, α, C_z and R respectively stand for the air density, the airfoil chord, the lift coefficient and the rotor radius. This simplified first aerodynamic model does not take into account the induced velocity, and the influence of the flap and lead-lag motions of blades are neglected. Aerodynamic drag forces on blades are also supposed to be negligible.

$$F_l = -\frac{1}{2}\cdot\rho\cdot\alpha\cdot C_z\cdot\theta\cdot\Omega^2\cdot\frac{R^3}{3} \qquad (22)$$

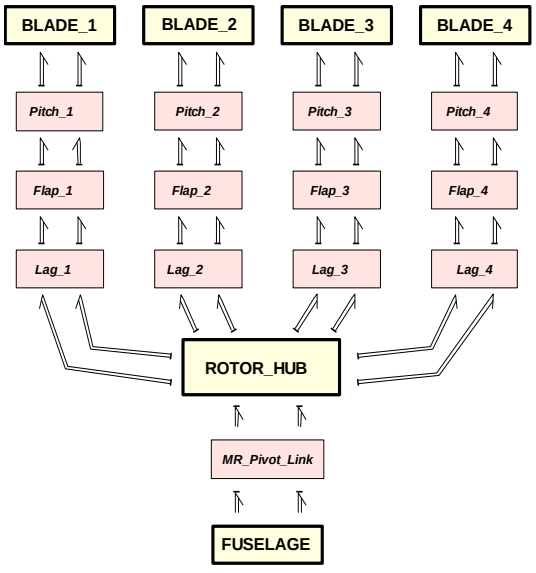

Figure 9. Word MBG of the rotor subsystem

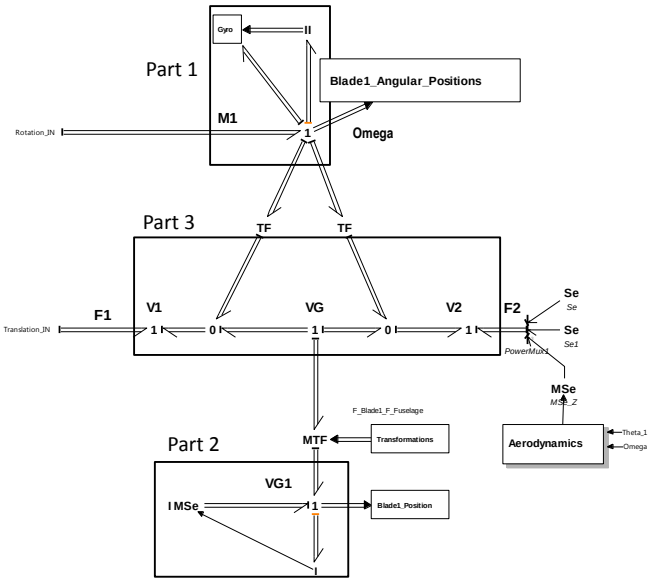

Figure 10. MBG of a moving rigid body - Example of a blade

The aerodynamic model do not appear in Figure 9 word MBG of the rotor since it has been included within each blade rigid body model, as depicted on the right hand side of Figure 10: A modulated effort source (MSe) generates the blade lift force on the third dimension of F2 force vector, while null forces are generated (Se and Se1 sources) for the x and y dimensions w-r-t the blade reference frame.

Through the example of one of the blades, Figure 10 gives the architecture of a rigid body multi-bond graph model based on [3]. The upper part 1 of the MBG represents the rotational dynamic behavior of the blade w-r-t its inertial coordinate frame, while the lower part 2 is for the translational motion of the blade center of mass w-r-t a fixed coordinate frame. The two corresponding '1' junctions correspond respectively to the rotational (Omega) and translational (VG1) velocity vectors expressed in these two coordinate frames. Both parts 1 and 2 are based on the Newton-Euler equations with respectively the blade inertia matrix (I1 element in part 1) associated with gyroscopic terms (Gyro) and the blade mass matrix (I element in part 2). The IMSe acting on the latter stands for Inertia Modulated effort Source and models the gravity effects applied to the blade center of mass. Part 3 describes the relations between the velocities V1 and V2 of the two hinge points of the blade and the velocity of the center of mass VG. These three velocity vectors are expressed in the body fixed coordinate frame. V1 corresponds to the velocity of the blade to hub joint, while V2 corresponds to the velocity of the point where the equivalent aerodynamic force F2 is applied (at 70% of the blade length from the hub). The two TF elements are the corresponding coordinate transformations between the body center of mass and these two points. The modulated transformation element (MTF) between VG1 and VG represents the coordinate transformation between the inertial coordinate frame and the body fixed reference frame.

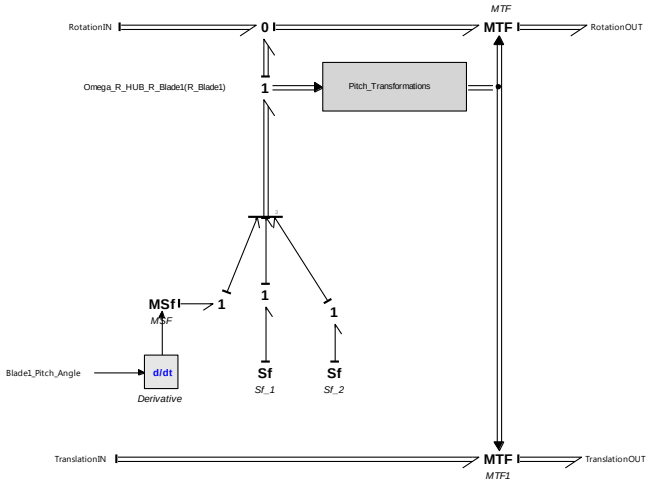

Figure 11. MBG representation of a joint - Case of a pitch pivot joint

Finally, external moments M1 and forces F1, appearing on the left hand side of this blade body representation, are respectively associated with velocities Omega and V1, and correspond to the rotational and translational output power bonds of one of the pitch pivot joints (see Figure 9).

The latter pitch pivot joint representation is given in Figure 11 as an example of joint multi-bond graph modeling. In this MBG, one can discern an upper part dedicated to the joint rotational degrees-of-freedom, while the lower part concerns the translational relations.

As the considered joint example corresponds to a pivot joint, the translational (lower) part consists in an integral transmission of the translational motion from the previous body or joint to the next body or joint – in the present case, from the previous flap pivot joint to the next blade body (see Figure 9) – through a coordinate transformation between the previous and the next elements coordinate frames. This modulated transformation (MTF) takes into account the relative angular position of the considered joint d-o-f. The rotational part of the pivot joint also uses this last coordinate transformation between the reference frames of the two considered elements and allows management of the joint rotational d-o-f. In the considered case, the pitch angle d-o-f of the joint is controlled by the blade pitch control subsystem acting as a modulated velocity source (MSf). Relative velocities of the two other dimensions are maintained to zero by null flow sources (Sf_1 and Sf_2).

SIMULATION RESULTS

To illustrate the bond graph tool ability to predict instability phenomena such as air resonance, the particular case of a stiff in-plane rigid rotor is considered. Air resonance conditions of occurrence have been discussed using an energy flow method in section 2, with a detailed explanation given in Appendix A for intersection of the body mode with the lead-lag mode in the two other branches of the air resonance diagram of Figure 1.

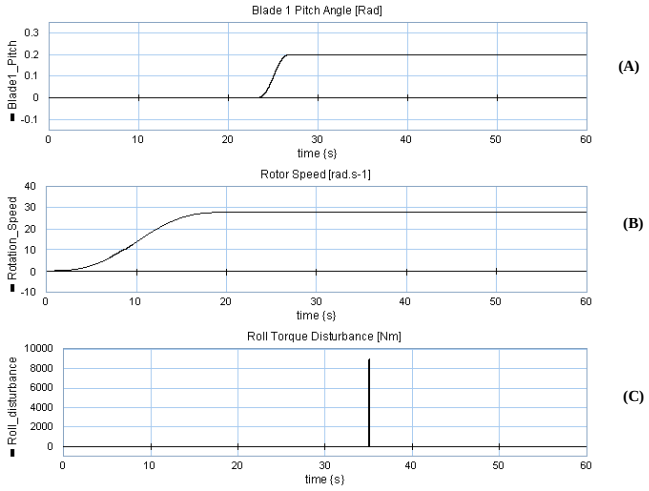

Figure 12. Preparatory simulation phase and torque disturbance pulse on the helicopter roll axis

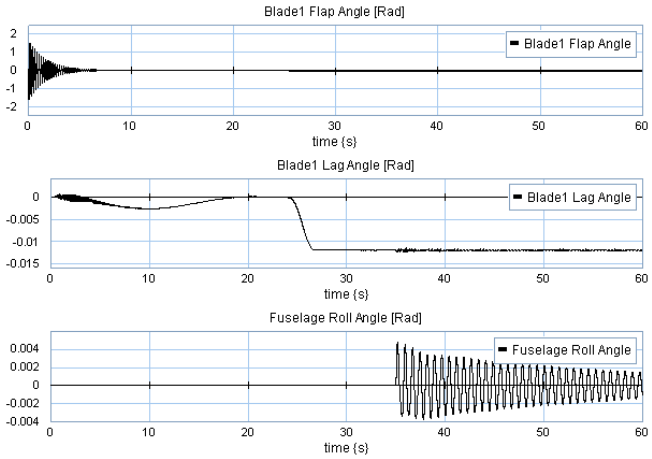

Figure 13. One blade flap (A) and lead-lag (B), and fuselage roll (B) responses to Figure 12 simulations conditions ($\omega_\zeta = 1.23{\cdot}\Omega_N$)

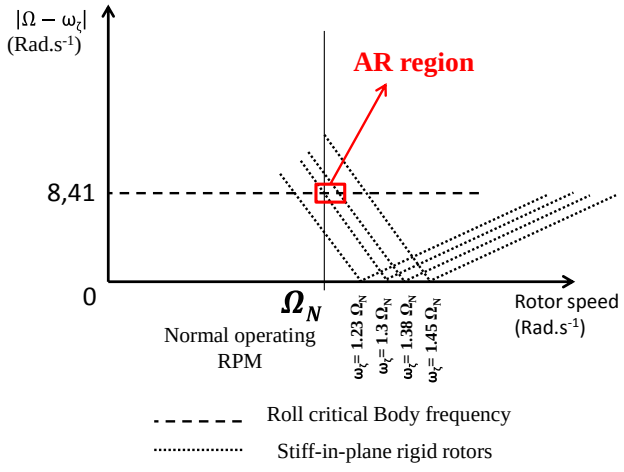

Figure 14. Air resonance diagram - case of stiff in-plane rotors

The multi-bond graph model exposed in the previous section has been prepared so as to reproduce a critical body frequency on the helicopter roll axis at $f_{Roll} = 1.34$ Hz, and the equivalent stiffness associated with each blade lead-lag joint is firstly tuned in order to simulate a stiff in-plane rotor with a lead-lag frequency at $\omega_\zeta = 1.23{\cdot}\Omega_N$, where Ω_N is the nominal operating rotor speed.

For simulation purpose, the 20Sim bond graph software is used with a backward differentiation method numerical integration.

As specific initial conditions calculations of each model body and joint would be a fastidious task for such a complicated 3-dimensional model with rotating bodies, all initial conditions are chosen to be null and a preparatory simulation phase is necessary to reach the desired operating conditions. This is illustrated in the simulation results exposed in Figure 12: The rotor is first accelerated to its nominal operating speed $\Omega_N = 27.75$ rad·s^{-1}, then the collective blade pitch angle is raised to $\theta_0 = 0.2$ rad so that a lift force is generated. These conditions are supposed to be equivalent to a hovering flight. Finally, a 9 kNm and 0.1 s torque disturbance is applied at 35 s on the helicopter fuselage roll axis in order to simulate a lateral wind gust. The resulting blade flap and lead-lag motions and helicopter body roll motion are given in Figure 13.

One can observe the oscillatory response of the fuselage roll with a $\omega_\zeta = 1.23{\cdot}\Omega_N$ lead-lag frequency, i.e., close to the air resonance region depicted in the air resonance diagram of Figure 14. Indeed, as exposed before, the AR is supposed to occur when $|\Omega - \omega_\zeta|$ is close to the roll critical body frequency $\omega_{Roll} = 8.41$ rad·s^{-1} when $\Omega = \Omega_N$. These coupling conditions are verified if $\omega_\zeta = 1.3{\cdot}\Omega_N$.

The lead-lag response when these theoretical conditions of air resonance occurrence are reached is given in Figure 15. Figure 16 and Figure 17 give respectively the lead-lag response when $\omega_\zeta = 1.38{\cdot}\Omega_N$ and $\omega_\zeta = 1.45{\cdot}\Omega_N$.

Concluding, the MBG model correctly predicted the appearance of the AR phenomena as the rotor lag was stiffened.

CONCLUSIONS

This paper proposes a complementary method to the usual ones for helicopters dynamics analysis. It is based on a structural and energetic vision and applied first to air resonance phenomena.

A global description of a helicopter is proposed using the word bond graph representation. Then a multi bond graph model of the main rotor and helicopter body subsystems are developed to address the AR phenomena. The model simulations are performed using the 20SIM software.

The simulation results of the MBG model show appearance of the AR phenomena and the impact of the lag stiffness value for stiff-in-plane rigid rotor.

Future work will consist in adapting this model to study other problems. For example: AR for soft-in-plane rigid rotor and for Ground resonance problem. Ambitions are also oriented to exploit the graphical aspect of the model in order to facilitate analysis of structural properties for controller design objectives.

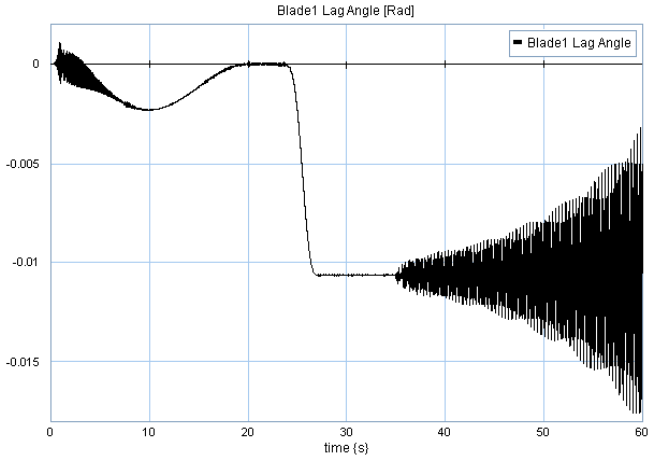

Figure 15. Lead-lag response when $\omega_\zeta = 1.3 \cdot \Omega_N$

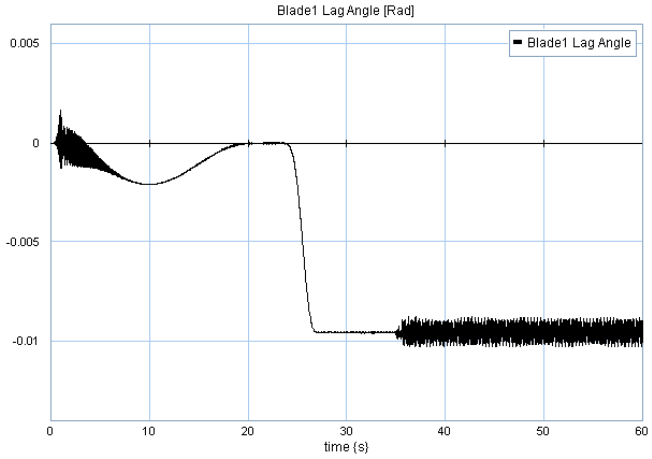

Figure 16. Lead-lag response when $\omega_\zeta = 1.38 \cdot \Omega_N$

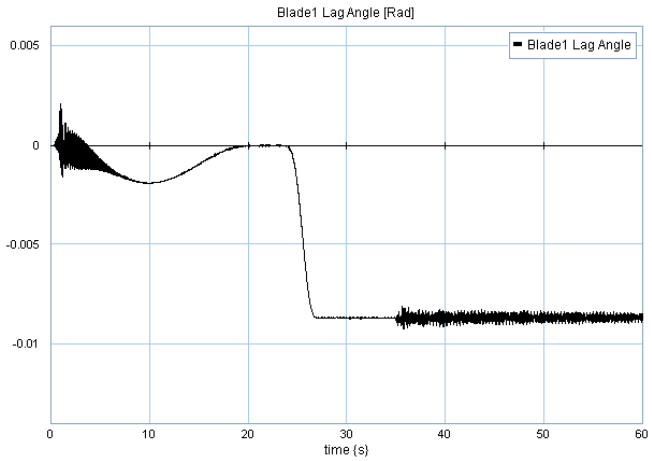

Figure 17. Lead-lag response when $\omega_\zeta = 1.45 \cdot \Omega_N$

APPENDIX A

Case 2

Consider next that the crossing of the shaft eigenfrequency with the regressing lead-lag mode occurs in point B, see Figure 18.

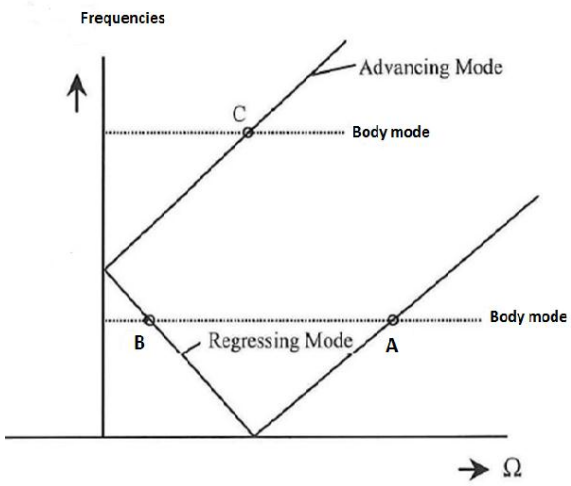

Figure 18. Diagram ground and air resonance

Assume also that the eigenfrequencies are:

$$\begin{aligned} \omega_\varsigma &= 2\Omega \\ \omega_{sh} &= \Omega \end{aligned} \tag{23}$$

The lead-lag motion as given by (12) becomes then:

$$\varsigma = \varsigma_0 \cos\left(\omega_\varsigma t\right) = \varsigma_0 \cos 2\psi \tag{24}$$

And the blade lead lag velocity and acceleration are:

$$\dot{\varsigma} = -\varsigma_0 \omega_\varsigma \sin\left(\omega_\varsigma t\right) = -2\varsigma_0 \Omega \sin 2\psi \tag{25}$$

$$\ddot{\varsigma} = -\varsigma_0 \omega^2_\varsigma \cos\left(\omega_\varsigma t\right) = -4\varsigma_0 \Omega^2 \cos 2\psi \tag{26}$$

Following the same procedure as above and describing first the lead-lag motion as an external excitation for the shaft, one can determine the effective forces on the hub due to the blade lead-lag motion as:

$$\begin{aligned} F_{xr} &= 2mR\Omega\dot{\varsigma} = -4mR\Omega^2\varsigma_0 \sin 2\psi \quad \text{(Coriolis)} \\ F_{yr} &= mR\left(\Omega^2\varsigma - \ddot{\varsigma}\right) = 5mR\Omega^2\varsigma_0 \cos 2\psi \quad \text{(Cf.+Inertia)} \end{aligned} \tag{27}$$

The first harmonic of the hub forces due to the blade lead-lag motion as seen by the shaft can be extracted by projecting these forces onto the shaft system of reference x0y0z0 as seen in Figure 19.

$$\begin{aligned} F_{x0} &= F_{xr}\cos\psi - F_{yr}\sin\psi = \frac{1}{2}mR\Omega^2\varsigma_0 \sin\psi - \frac{9}{2}mR\Omega^2\varsigma_0 \sin 3\psi \\ F_{y0} &= F_{xr}\sin\psi + F_{yr}\cos\psi = \frac{1}{2}mR\Omega^2\varsigma_0 \cos\psi + \frac{9}{2}mR\Omega^2\varsigma_0 \cos 3\psi \end{aligned} \tag{28}$$

Using (24) and (27), the 1st harmonic on the shaft can be represented as seen in Figure 20.

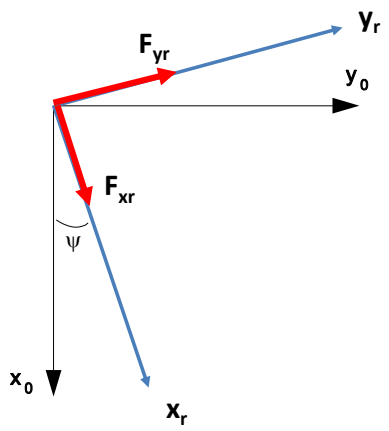

Figure 19. Projection of hub forces induced by lead-lag motion on the shaft

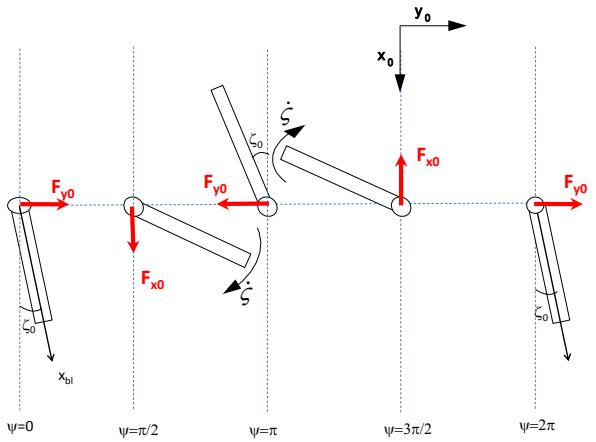

Figure 20. Lead-lag motion of one blade as external excitation for the shaft and the corresponding force on the shaft, Case 2

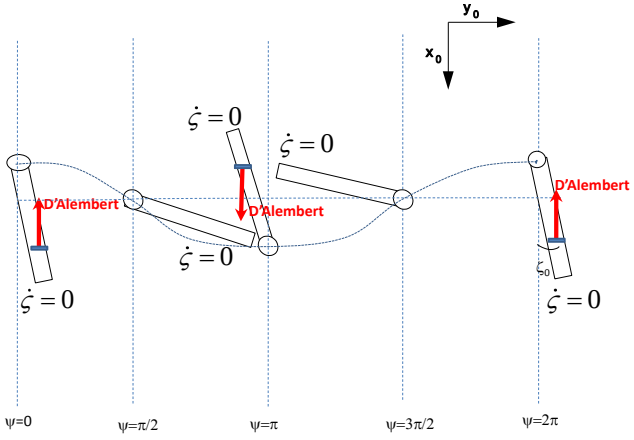

Figure 21. Longitudinal shaft motion as external excitation for the blade and the corresponding force on the blade, Case 2

Describe next the shaft motion as an external excitation for the blades. Assume that the shaft can move only longitudinally (direction x0), being excited in its eigenfrequency $\omega_{sh}=\Omega$. The blades will move up and down with the shaft with an acceleration $\ddot{x}_{sh}$. Looking at (24), the shaft longitudinal displacement will be:

$$x_{sh}=x_{sh0}\cos\left(\omega_{sh}t\right)=x_{sh0}\cos\psi \tag{29}$$

The force on blade due to the shaft motion is according to D'Alembert principle:

$$f=-f_0\cos\psi \tag{30}$$

and the motion of the shaft during one rotor revolution is represented as seen in Figure 21.

The extra lead-lag moment due to the longitudinal shaft motion can be calculated as:

$$\begin{aligned} M=-fR\sin\left(\psi+\varsigma\right) &\overset{\text{linearized}}{\approx} f_0R\cos\left(\psi\right)\left(\sin\psi+\varsigma\cos\psi\right)= \\ f_0R\cos\left(\psi\right)&\left(\sin\psi+\varsigma_0\cos\left(2\psi\right)\cos\psi\right)= \\ f_0R\frac{1}{2}\sin 2\psi &+ f_0\varsigma_0R\left(\frac{1}{2}\cos 3\psi+\frac{1}{2}\cos\psi\right) \end{aligned} \tag{31}$$

One can see that (31) is out of phase with lag velocity (25), thus there is no energy passing from the shaft to the blades. Also, from (28) and (29), one can see that Fx0 is out of phase with $\dot{x}_{sh}$, thus no energy input goes from the blades to the shaft.

Assuming next that the shaft can move only laterally (direction y0) and following the procedure explained above, the shaft lateral displacement can be described as:

$$x_{sh}=x_{sh0}\sin\left(\omega_{sh}t\right)=x_{sh0}\sin\psi \tag{32}$$

The force on blade due to the shaft motion is according to D'Alembert principle:

$$f=-f_0\sin\psi \tag{33}$$

and the lateral motion of the shaft during one rotor revolution is represented as seen in Figure 22.

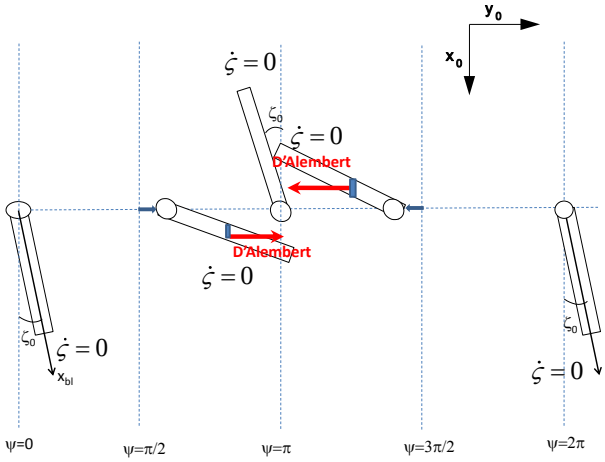

Figure 22. Lateral shaft motion as external excitation for the blade and the corresponding force on the blade, Case 2

The extra lead-lag moment due to the lateral shaft motion can be calculated as:

$$M = fR\cos(\psi+\varsigma) \overset{\text{linearized}}{\approx} f_0 R\sin\psi(\cos\psi+\varsigma\sin\psi) = f_0 R\sin\psi(\cos\psi-\varsigma_0\cos(2\psi)\sin\psi) = f_0 R\frac{1}{2}\sin 2\psi - f_0\varsigma_0 R\left(\frac{1}{2}\cos 2\psi - \frac{1}{4} - \frac{1}{4}\cos 4\psi\right) \quad (34)$$

One can see that (34) is also out of phase with lag velocity (25), thus there is no energy passing from the shaft to the blades. Also, from (28) and (32) one can see that Fy0 is in phase with $\dot{x}_{sh}$, thus there is energy input going from the blades to the shaft. However, as no energy goes back from the shaft to the blades, this part of the regressing lead-lag mode branch as seen in Figure 18 is not dangerous for air/ground resonance instability as driving energy is not available.

Case 3

Finally, consider that the crossing of the shaft eigenfrequency with the advancing lead-lag mode occurs in point C, see Figure 18. Assume also that the eigenfrequencies are:

$$\omega_\varsigma = \Omega \qquad \omega_{sh} = 2\Omega \quad (35)$$

The assumed oscillatory lead-lag motion is then:

$$\varsigma = \varsigma_0\cos(\omega_\varsigma t) = \varsigma_0\cos\psi \quad (36)$$

And the blade lead lag velocity and acceleration are:

$$\dot{\varsigma} = -\varsigma_0\omega_\varsigma\sin(\omega_\varsigma t) = -\varsigma_0\Omega\sin\psi \quad (37)$$

$$\ddot{\varsigma} = -\varsigma_0\omega_\varsigma^2\cos(\omega_\varsigma t) = -\varsigma_0\Omega^2\cos\psi \quad (38)$$

Describe first the lead-lag motion as an external excitation for the shaft, one can determine the effective forces on the hub due to the blade lead-lag motion as:

$$F_{xr} = 2mR\Omega\dot{\varsigma} = -2mR\Omega^2\varsigma_0\sin\psi \quad \text{(Coriolis)}$$
$$F_{yr} = mR(\Omega^2\varsigma - \ddot{\varsigma}) = 2mR\Omega^2\varsigma_0\cos\psi \quad \text{(Cf.+Inertia)} \quad (39)$$

The hub forces due to the blade lead-lag motion as seen by the shaft are obtained using (28) and Figure 19 as:

$$F_{x0} = F_{xr}\cos\psi - F_{yr}\sin\psi = -2mR\Omega^2\varsigma_0\sin 2\psi$$
$$F_{y0} = F_{xr}\sin\psi + F_{yr}\cos\psi = 2mR\Omega^2\varsigma_0\cos 2\psi \quad (40)$$

Using (36) and (40), the shaft forces and the blade motion can be represented as seen in Figure 23.

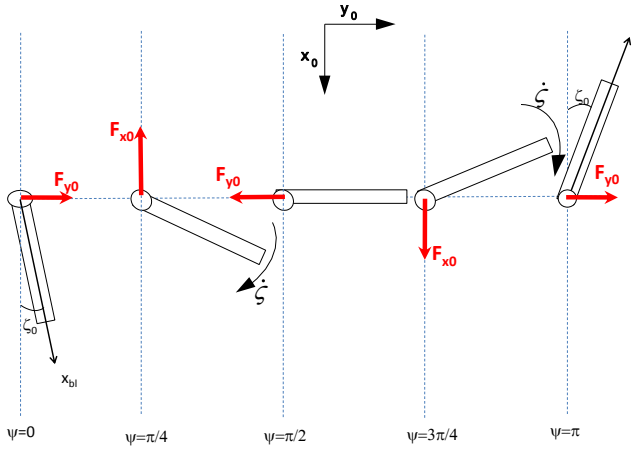

Figure 23. Lead-lag motion of one blade as external excitation for the shaft and the corresponding force on the shaft, Case 3

Describe next the shaft motion as an external excitation for the blades. Assume that the shaft can move only longitudinally (direction x0), being excited in its eigenfrequency $\omega_{sh} = \Omega$. The blades will move up and down with the shaft with an acceleration $\ddot{x}_{sh}$. Looking at (36), the shaft longitudinal displacement will be:

$$x_{sh} = x_{sh0}\cos(\omega_{sh} t) = x_{sh0}\cos 2\psi \quad (41)$$

The force on blade due to the shaft motion is according to D'Alembert principle:

$$f = -f_0\cos 2\psi \quad (42)$$

and the motion of the shaft during one rotor revolution is represented as seen in Figure 24.

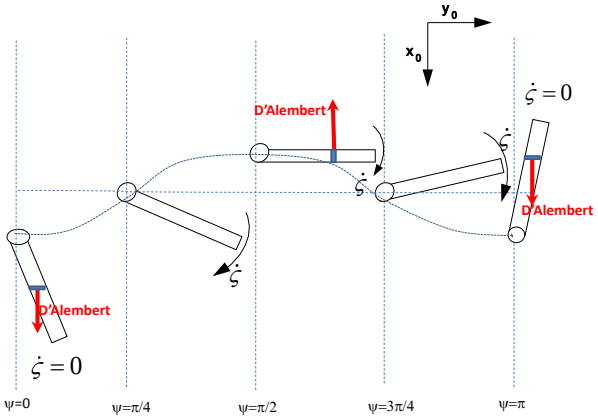

Figure 24. Longitudinal shaft motion as external excitation for the blade and the corresponding force on the blade, Case 3

The extra lead-lag moment due to the longitudinal shaft motion can be calculated as:

$$M = -fR\sin(\psi+\varsigma) \overset{\text{linearized}}{\approx} -f_0 R\cos(2\psi)(\sin\psi+\varsigma\cos\psi) = -f_0 R\cos(2\psi)(\sin\psi+\varsigma_0\cos^2\psi) = -f_0 R\left(\frac{1}{2}\sin 3\psi - \frac{1}{2}\sin\psi\right) - f_0\varsigma_0 R\left(\frac{1}{4}+\frac{1}{2}\cos 2\psi + \frac{1}{4}\cos 4\psi\right) \quad (43)$$

One can see that (43) is out of phase with lag velocity (37), thus there is no energy passing from the shaft to the blades. Also, from (41) and (40), one can see that Fx0 is in phase with $\dot{x}_{sh}$, thus energy input goes from the blades to the shaft.

Assuming next that the shaft can move only laterally (direction y0) and following the procedure explained above, the shaft lateral displacement can be described as:

$$x_{sh} = x_{sh0} \sin(\omega_{sh} t) = x_{sh0} \sin 2\psi \tag{44}$$

The force on blade due to the shaft motion is according to D'Alembert principle:

$$f = -f_0 \sin 2\psi \tag{45}$$

and the lateral motion of the shaft during one rotor revolution is represented as seen in Figure 25.

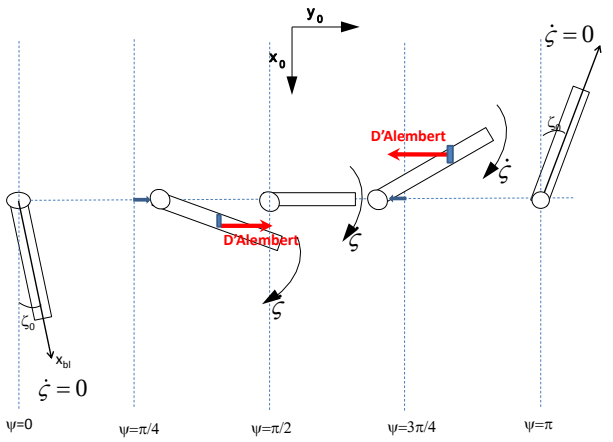

Figure 25. Lateral shaft motion as external excitation for the blade and the corresponding force on the blade, Case 3

The extra lead-lag moment due to the lateral shaft motion can be calculated as:

$$\begin{aligned} M = fR\cos(\psi+\varsigma) &\overset{\text{linearized}}{\approx} f_0 R \sin 2\psi (\cos\psi - \varsigma \sin\psi) = \\ f_0 R \sin 2\psi (\cos\psi - \varsigma_0 \sin\psi \cos(2\psi)) &= \\ f_0 R\left(\frac{1}{2}\sin 3\psi + \frac{1}{2}\sin\psi\right) - f_0 \varsigma_0 R\left(\frac{1}{4} - \frac{1}{4}\cos 2\psi\right) & \end{aligned} \tag{46}$$

One can see that (46) contains one component out of phase with lag velocity (37), thus there is no energy passing from the shaft to the blades. Therefore, the advancing lead-lag mode branch of Figure 18, although contains driving energy, the vicious circle of energy flow from the blade lead-lag motion to the shaft motion and back is not closed. Therefore the advancing lead-lag mode is not involved in air and ground resonance instability. Reference [13] demonstrated the a case at a 2-bladed wind turbine where the vicious circle was closed by the advancing lead-lag mode, the problem was the gravity force which was enabling the "pumping" of energy from blade to shaft and back.

ACKNOWLEDGMENTS

This work was supported by the "Complex Mechanical Systems Dynamics" project - EADS Foundation - Arts et Metiers Paritech - Ecole Centrale de Marseille.

REFERENCES

[1] H. M. Paytner, "Analysis and Design of Engineering systems", MIT-Press, Camb, MA, 1961.

[2] D. C. Karnopp, D. L. Margolis, R. C. Rosemberg, "System Dynamics - Modeling and Simulation of Mechatronic Systems", Wiley Interscience, ISBN 0-471-33301-8, 3rd iss. 2000.

[3] W. Borutzky "Bond Graph Methodology: Development and Analysis of Multidisciplinary Dynamic System Models", Springer, ISBN: 1848828829 9781848828827, 2010.

[4] Donham, R. E.; Cardinale, S. V.; Sachs I.B., Ground and Air Resonance Characteristics of a Soft In-Plane Rigid-Rotor System, Journal of the American Helicopter Society, Volume 14, Number 4, 1 October 1969 , pp. 33-41

[5] Zhang Xiao-gu, Physical Understanding of Helicopter Air and Ground Resonance, Journal of the American Helicopter Society, Vol. 31, No. 4, October 1986 , pp. 4-11,

[6] Ormiston, Robert, A, Rotor-Fuselage Dynamics of Helicopter Air and Ground Resonance, Journal of the American Helicopter Society, Vol. 36, No. 2, April 1991 , pp. 3-20].

[7] T. Krysinski, F. Malburet, "Mechanical Instability", Wiley. ISBN: 978-1-8482-1201-5, 2011.

[8] A. R. S. Bramwell "An Introduction to Helicopter Air Resonance", The City University, London. Reports and Memoranda No. 3777. September, naca.central.cranfield.ac.uk/reports/arc/rm/3777.

[9] H. YEO, I. Chopra "Coupled rotor/fuselage vibration analysis using detailed 3-D airframe models", Mathematical and Computer Modelling: An International Journal, Volume 33 Issue 10-11, May, 2001, Pages 1035-1054.

[10] P. Masarati, V. Muscarello, G. Quaranta, "Robust aeroservoelastic stability of helicopters: application to the air/ground resonance", American Helicopter Society 67th Annual Forum, Virginia Beach, VA, May 3–5, 2011

[11] C. S. Robinson, R. Wood, R. L. King, "Full Nonlinear Simulation of Coupled Rotor/Fuselage Response Using Symbolically Derived Equations of Motion", American Helicopter Society 54th Annual Forum, Washington D.C, May 20–22, 1998.

[12] Bielawa, Richard L., Rotary wing structural dynamics and aeroelasticity, American Institute of Aeronautics and Astronautics, Jan. 2006.

[13] Pavel, M.D., Modeling Lead-Lag Dynamics for Rotorcraft-Pilot-Couplings Investigation, American

Helicopter Society 66th Annual Forum & Technology Display, May 11-13, 2010, Phoenix Arizona

[14] Burkam, John E.; Miao, Wen-Liu, Exploration of Aeroelastic Stability Boundarieswith a Soft-in-Plane Hingeless-Rotor Model, Journal of the American Helicopter Society, Volume 17, Number 4, 1 October 1972 , pp. 27-35Burkam and Miao, 1972

[15] Lantzsch, Robin, Wolfram Jens, Mario Hamers, "Increasing Handling Qualities and Flight Control Performance using an Air Resonance Controller", 64th Annual Forum of the American Helicopter Society, Montreal, Canada, April 29-May 1, 2008Lantzsch, Wolfram and Hamers, 2008

[16] J. van Amerongen, P. Breedveld, "Modelling of Physical Systems for the Design and Control of Mechatronic Systems", Annual Reviews in Control, Volume 27, Issue 1, 2003, pp. 87-117, ISSN 1367-5788, 10.1016/S1367-5788(03)00010-5.

[17] W. Borutzky, "Bond Graph Modelling and Simulation of Multidisciplinary Systems – An Introduction, Simulation Modelling", Practice and Theory, Volume 17, Issue 1, January 2009, Pages 3-21, ISSN 1569-190X, 10.1016/j.simpat.2007.08.008.

[18] Q. Zhao, F. Gao, "Bond graph modelling of hydraulic six-degree-of-freedom motion simulator" Proceedings of the Institution of Mechanical Engineers, Part C: Journal of Mechanical Engineering Science, December 2012 , vol. 226 no. 12 2887-2901.

[19] L.S. Bonderson, "Vector bond graphs applied to one-dimensional distributed systems",. Journal of Dynamic Systems, Measurement and Control, pages 75–82, 1975.

[20] P.C. Breedveld." Multibond Graph Elements in Physical Systems" Theory. Journal of the Franklin Institute, 319(1/2):1–36, 1985.

[21] M.J.L. Tiernego and A.M. Bos, "Modelling the dynamics and kinematics of mechanical systemswith multibond graphs", Journal of the Franklin Institute, 319(1/2):pp. 37–50, 1985.

[22] S. Behzadjpour, A. Khajepour, "Causality in vector bond graphs and its application to modeling of multi-body dynamic systems", Simulation Modelling Practice and Theory 14 (2006) 279–295.

[23] R. Cacho, J. Felez, C. Vera, "Deriving simulation models from bond graphs with algebraic loops. The extension to multibond graph systems", Journal of the Franklin Institute 337 (2000) 579-600.

[24] Luis I. Silva, Guillermo A. Magallan, Pablo M. de la Barrera, Cristian H. De Angelo and Guillermo O. Garcia "Modeling of Electric Vehicles Dynamics with Multi-Bond Graphs" Vehicle Power and Propulsion Conference (VPPC), Lille, 1-3 September 2010.

[25] A. Vas, S. Hirai, "Application of Vector Bond Graphs to the Modeling of a Class Hand Prostheses", Proceedings of ESDA04, 7th Biennial ASME Conference on Engineering Systems Design and Analysis, July 19-22, 2004, Manchester, United Kingdom.

[26] M. Raju Hossain, D. Geoff Rideout, and D. Nicholas Krouglicof, "Bond graph dynamic modeling and stabilization of a quad-rotor helicopter", Proceedings of Spring Simulation Multiconference (SpringSim '10). Society for Computer Simulation International, San Diego, CA, USA, 2010, Article 215, 7 pages.

[27] Martinez, M. L. and Romero, G. and Maroto, J. and Felez, J.," Simulation Model of the Scanner Servocontrols for the Orientation of a Fighter Aircraft by Using the Bond Graph Technique", Computational Intelligence, Communication Systems and Networks (CICSyN), Second International Conference on, July 2010, pages 106-111.